Electronic Supporting Information

NiCo/NiO-CoO_x Ultrathin Layered Catalyst with Strong Basic Sites for High-Performance H_2 Generation from Hydrous Hydrazine

Dandan Wu [a], Ming Wen*[a,b], Xijian Lin[a], Qingsheng Wu[a], Chen Gu[a] and Hanxing Chen[a]

[a]Department of Chemistry, Shanghai Key Laboratory of Chemical Assessment and Sustainability, Tongji University, 1239 Siping Road, Shanghai 200092, R. P. China.
[b]Shanghai Key Laboratory of D&A for Metal-Functional Materials, Tongji University, 4800 Caoan Road, Shanghai 201804, China.

Corresponding Authors

*Ming Wen: E-mail: m_wen@tongji.edu.cn.

The Supplement of Experimental Section

1. Chemicals

All chemicals were commercial and used without further purification. Nickel chloride hexahydrate ($NiCl_2·6H_2O$, Sinopharm Chemical Reagent Co., Ltd., ≥98%), cobalt chloride hexahydrate ($CoCl_2·6H_2O$, Aladdin Chemistry Co., Ltd, ≥99.7%), hydrazine monohydrate ($N_2H_4·H_2O$, Aladdin Chemistry Co., Ltd, 98%), potassium borohydride (KBH_4, shanghai Mackin Biochemical Co., Ltd., 97%), sodium carbonate (Na_2CO_3, Sinopharm Chemical Reagent Co., Ltd., ≥99.8%), ethanol absolute (C_2H_5OH, Sinopharm Chemical Reagent Co., Ltd., ≥99.7%), hydrochloric acid (HCl, Sinopharm Chemical Reagent Co., Ltd., 37%), γ Aluminium oxide (γ-Al_2O_3, Aladdin Chemistry Co., Ltd, 99.99%), Collodion were purchased from Shanghai Ling feng Chemical Reagent Co. Ltd..

2. Synthesis of NiCo/NiO-CoO_x catalysts with different of NiCo content

In a typically method, When the morphology is urchin-like spheres and nanosheets, we can obtain the composite catalysts with different content of NiCo by changing the incomplete precipitate time (10 min, 15 min, 20 min and 25 min is named as S-a, S-b, S-c and S-d, respectively), or by changing the volume of injected Na_2CO_3 when the morphology is NPs.

3. Synthesis of NiO-CoO_x catalysts

Following the analogous synthetic process of $Ni_{70}Co_{30}$/NiO-CoO_x nanosheets, urchin-like spheres and NPs catalysts but without the reduction step and let them precipitate completely, then calcine in argon at 400 °C for 1 h with a heating rate of 1 °C min^{-1} can obtain NiO-CoO_x with corresponding morphology.

4. Synthesis of $Ni_{70}Co_{30}$ NPs

An aqueous solution of potassium borohydride (25 mL, 25 mM) was added into 100mL solution of a $NiCl_2$ (25 mM) and $CoCl_2$ (25 mM) mixture in a molar ratio of 7:3 under magnetic stirring within 20 min at 0 °C. The final precipitate was filtered, washed thoroughly with deionized water and dried at 60 °C for 24 h. Then the as-

obtained precipitate was calcined in argon at 400 °C for 1 h with a heating rate of 1 °C min^{-1} to get $Ni_{70}Co_{30}$ NPs.

5. Synthesis of $Ni_{70}Co_{30}/Al_2O_3$ catalyst.

3 g γ-Al_2O_3 were dissolved in 100 mL solution of $NiCl_2$ (25 mM) and $CoCl_2$ (25 mM) mixture in a molar ratio of 7:3 by magnetic stirring, to which an aqueous solution of potassium borohydride (25 mL, 25 mM) was added within 20 min at 0 °C. The final precipitate was filtered, washed thoroughly with deionized water and dried at 60 °C for 24 h. Then the as-obtained precipitate was calcined in argon at 400 °C for 1h with a heating rate of 1 °C min^{-1} to get $Ni_{70}Co_{30}/Al_2O_3$ catalysts.

6. CO_2 TPD Experiment

CO_2 temperature-programmed desorption (TPD) was carried out as follows. First, the air on the sample surface was removed under an argon stream (purity of 99.999%) at 573 K for 1 h and the surface was cooled to room temperature in the same argon stream. Then, CO_2 was preadsorbed by the catalyst at 323 K for 2 h. The CO_2 stream was then replaced with the carrier gas, which was kept at 323 K for 2h to purge the gas and physically absorbed CO_2 away from the catalyst surface. After the surface was cooled down to room temperature, CO_2 desorption was carried out by raising the temperature at a speed of 10 K min^{-1} up to 1073 K, and the released CO_2 was determined by an on-line gas chromatograph equipped with a thermal conductivity detector.

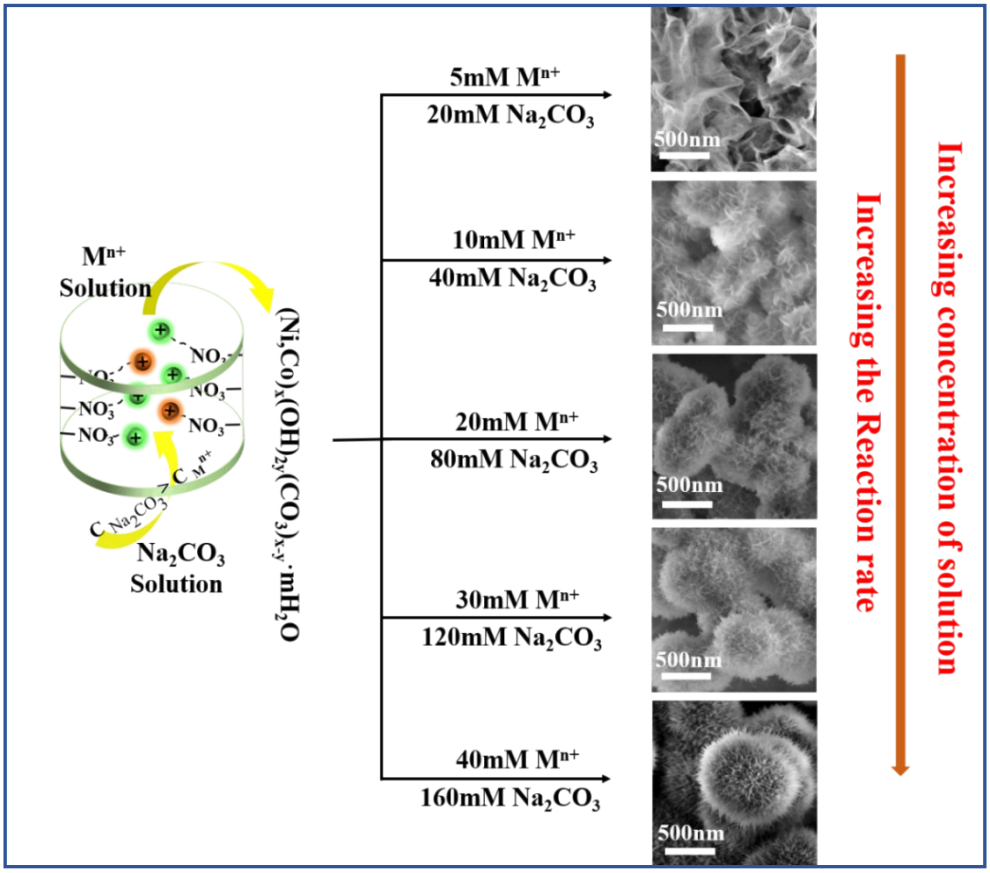

Figure S1. Scheme of the effect of the solution concentration on the synthesis of subcarbonate precursor

As show in Figure S1, the influence of reaction system concentration on the morphology of $(Ni,Co)_x(OH)_{2y}(CO_3)_{x-y}\cdot mH_2O$ has been studied in detail. The increase of solution concentration raises the reaction velocity in the dynamic controlling process, and thereby the morphology gradually changes from nanosheet to urchin-like sphere.

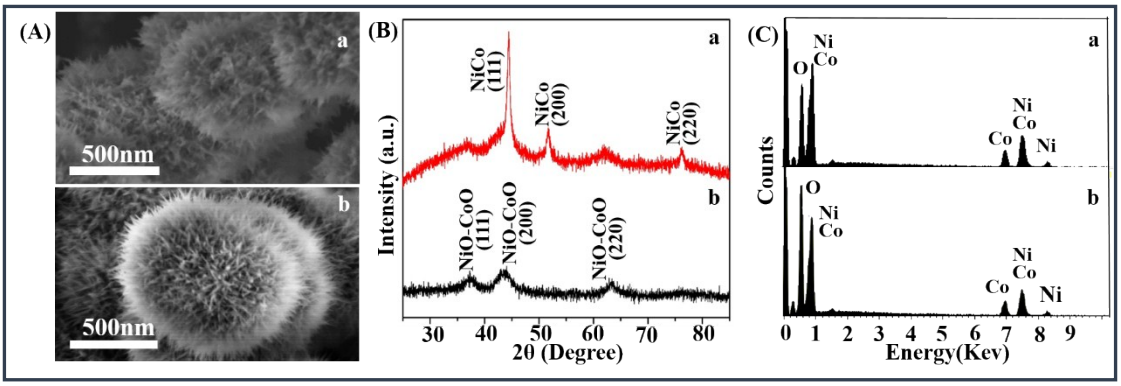

Figure S2. SEM images (A), XRD patterns (B) and EDS analysis (C) of urchin-like NiCo/NiO-CoO_x (a) and NiO-CoO_x (b).

Figure S2 shows the morphology characterization and structure analysis of urchin-like NiO-CoO_x and NiCo/NiO-CoO_x. It can be observed that NiCo NPs are all uniformly anchored on the surface of urchin-like NiO-CoO_x spheres in SEM images (Figure S2A). The XRD pattern of NiO-CoO_x (Figure S2 Bb) shows three broad peaks, and all the diffraction peaks (37.0° (111), 42.9° (200) and 62.0° (220)) between the cubic NiO phase (space group: Fm-3m; JCPDS#65-2901) and the cubic CoO phase (space group: Fm-3m; JCPDS#65-2902). The pattern of NiCo/NiO-CoO_x nanocomposite (Figure S2 Ba) has three sharp peaks at 44.3° (111), at 51.6° (200) and at 76.0° (220) besides the peaks of NiO-CoO_x, which indicates the formation of NiCo solid solution and agrees well with the face-centered cubic (fcc) lattice of Ni (JCPDF#65-0380) and Co (JCPDF#15-0806), further confirming the fabrication of heterostructured NiCo/NiO-CoO_x nanocomposites. The EDS analysis performed separately on urchin-like spheres of NiCo/NiO-CoO_x (Figure S2 Ca) and NiO-CoO_x (Figure S2 Cb) prove that both of them contain Ni, Co, and O. The atomic ratio of Ni:O and Co:O increase a little after anchoring NiCo on the surface of NiO-CoO_x, again certifying the formation of NiCo/NiO-CoO_x composite. Thus the present coprecipitation-reduction method is highly effective to obtain the heterostructured urchin-like NiCo/NiO-CoO_x nanocomposites with NiCo NPs uniformly loaded on the surface of urchin-like NiO-CoO_x spheres.

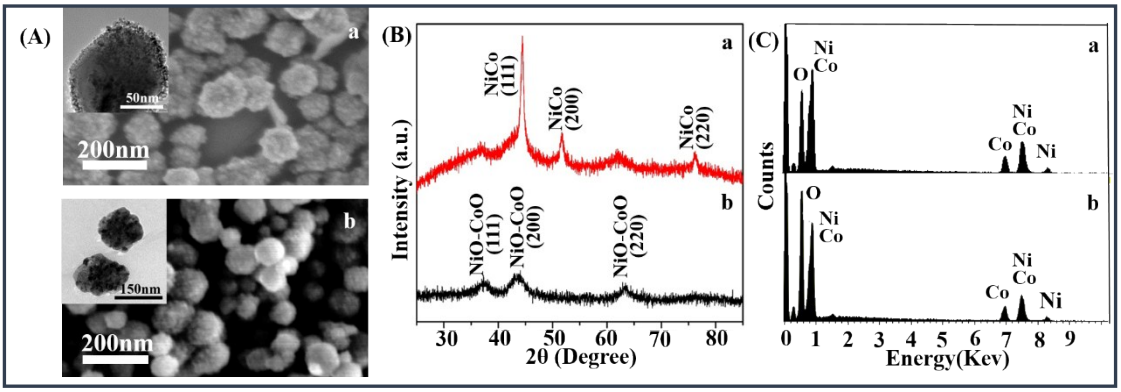

Figure S3. SEM images (A) with inset of TEM images, XRD patterns (B) and EDS analysis (C) of NiCo/NiO-CoO_x NPs(a) and NiO-CoO_x NPs(b).

The morphology characterization and structure analysis of NiO-CoO_x NPs and NiCo/NiO-CoO_x NPs are given in Figure S3. It can be observed that NiCo NPs are all uniformly anchored on the surface of NiO-CoO_x NPs (Figure S3A). The XRD pattern of NiO-CoO_x (Figure S3 Bb) shows three broad peaks, and all the diffraction peaks (37.0° (111), 42.9° (200) and 62.0° (220)) between the cubic NiO phase (space group: Fm-3m; JCPDS#65-2901) and the cubic CoO phase (space group: Fm-3m; JCPDS#65-2902). The pattern of NiCo/NiO-CoO_x nanocomposite (Figure S3 Ba) has three sharp peaks at 44.3° (111), at 51.6° (200) and at 76.0° (220) besides the peaks of NiO-CoO_x, which indicates the formation of NiCo solid solution and agrees well with the fcc lattice of Ni (JCPDF#65-0380) and Co (JCPDF#15-0806), further confirming the fabrication of heterostructured NiCo/NiO-CoO_x nanocomposites. The EDS analysis performed separately on NiCo/NiO-CoO_x NPs (Figure S3 Ca) and NiO-CoO_x NPs (Figure S3 Cb) prove that both of them contain Ni, Co, and O. And the atomic ratio of Ni:O and Co:O increase a little after anchoring NiCo on the surface of NiO-CoO_x NPs, again certifying the formation of NiCo/NiO-CoO_x composite. Thus the present DCCR method is highly effective to obtain the heterostructured NiCo/NiO-CoO_x nanocomposites with NiCo NPs uniformly loaded on the surface of NiO-CoO_x NPs.

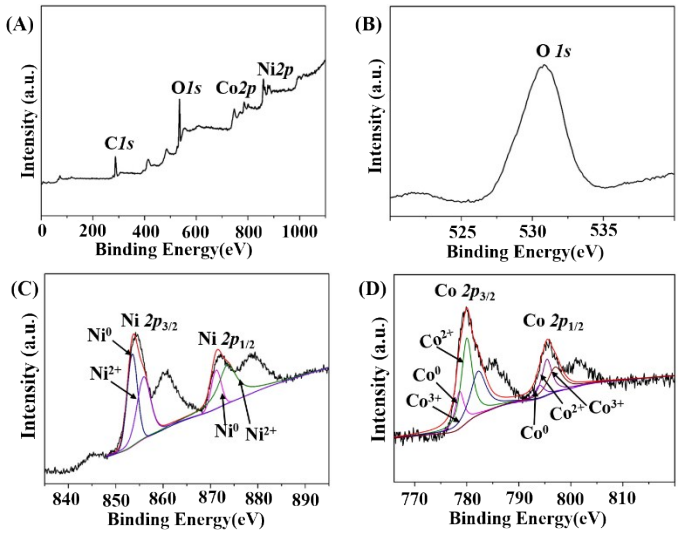

Figure S4. (A) XPS analysis of urchin-like NiCo/NiO-CoO_x and detailed analysis of O1*s* (B), Ni 2*p*(C) and Co 2*p* (D) from urchin-like NiCo/NiO-CoO_x.

XPS was measured to explore the surface element valance information of urchin-like NiCo/NiO-CoO_x. In Figure S4, the numbers of emitted photoelectrons are given as a function of binding energy up to 1100 eV. Four photoemission peaks (Ni *2p*, Co *2p*, O *1s* and C *1s*) appear in the wide spectra of the urchin-like NiCo/NiO-CoO_x (Figure S4A). The detailed spectrum of Ni *2p* peaks magnified from the wide spectrum of the urchin-like NiCo/NiO-CoO_x shows two peaks at 854.2 eV and 871.5 eV due to the spin–orbit splitting of $2p_{3/2}$ and $2p_{1/2}$, respectively, and two satellite peaks at 860.8 and 880.1 eV are two shakeup type peaks of nickel at the high binding energy side of Ni $2p_{3/2}$ and Ni $2p_{1/2}$. In order to clarify the exact bonding form of Ni, the narrow Ni spectrum was analyzed by using XPSPEAK41 software. As shown in Figure S4C the peak of Ni $2p_{3/2}$ and Ni $2p_{1/2}$ both can be split to two peaks with BE values of 853.5 eV & 855.9 eV and 871.2 eV & 873.6 eV, attributed to Ni (0) and Ni (II). The detailed spectrum of Co *2p* peaks in Figure S4D are analogous to Ni *2p* peaks, and the peaks of Co $2p_{3/2}$ and Co$2p_{1/2}$ both can be split to three peaks with BE values of 778.2, 780, 782.9 eV, and 794.1, 795.4, 798 eV, respectively, correspond to Co (0) , Co (II) and Co (III). As a trace of Co (II) in the catalyst surface can be oxidized to Co (III) in the process of sample storage and characterization, Co (III) can be observed. Furthermore, in Figure S4B the O *1s* peak at 530.5 eV indicates the presence of the O species existing in the Ni–O bonds in NiO and Co–O bonds in CoO_x (Figure S4B).

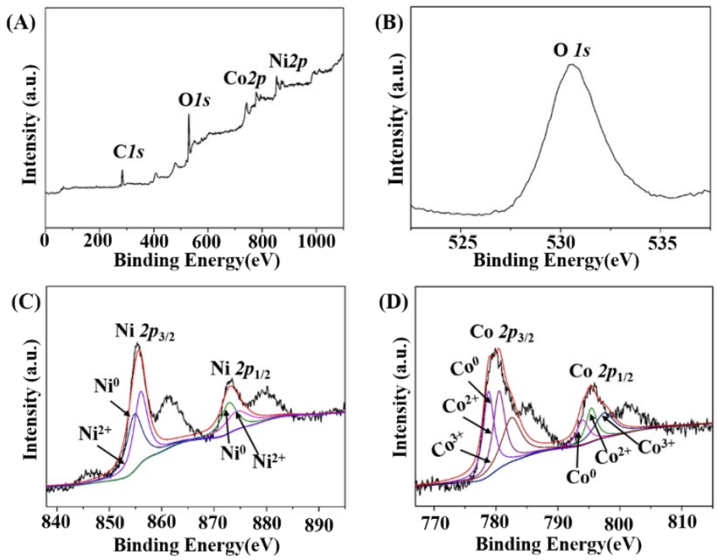

Figure S5. (A) XPS analysis of NiCo/NiO-CoO_x NPs and detailed analysis of O*1s* (B), Ni *2*p(C) and Co *2p*(D) from NiCo/NiO-CoO_x NPs.

Figure S5 shows the XPS analysis of NiCo/NiO-CoO_x NPs, in which the numbers of emitted photoelectrons are given as a function of binding energy up to 1100 eV. Four photoemission peaks (Ni *2p*, Co *2p*, O *1s* and C *1s*) appear in the wide spectra of the NiCo/NiO-CoO_x NPs (Figure S5A). The detailed spectrum of Ni *2p* peaks magnified from the wide spectrum of the NiCo/NiO-CoO_x NPs shows two peaks at 854.8 eV and 872.1 eV due to the spin–orbit splitting of $2p_{3/2}$ and $2p_{1/2}$, respectively, and two satellite peaks at 861 and 880.6 eV are two shakeup type peaks of nickel at the high binding energy side of Ni $2p_{3/2}$ and Ni $2p_{1/2}$. And the narrow Ni spectrum was further analyzed by using XPSPEAK41 software to clarify the exact bonding form of Ni. As shown in Figure S5C the peak of Ni $2p_{3/2}$ and Ni $2p_{1/2}$ both can be split to two peaks with BE values of 854.5 eV & 856 eV and 872.8 eV & 874.3 eV, attributed to Ni (0) and Ni (II). The detailed spectrum of Co *2p* peaks in Figure S4D are analogous to Ni *2p* peaks, and the peaks of Co $2p_{3/2}$ and Co$2p_{1/2}$ both can be split to three peaks with BE values of 778.8, 780.5, 782.5 eV, and 794, 795.4, 797.5 eV, respectively, correspond to Co (0) , Co (II) and Co (III). As a trace of Co (II) in the catalyst surface can be oxidized to Co (III) in the process of sample storage and characterization, Co (III) can be observed. Moreover, the O *1s* peak at 530.3 eV indicates the presence of the O species existing in the Ni–O bonds in NiO and Co–O bonds in CoOx (Figure S5B).

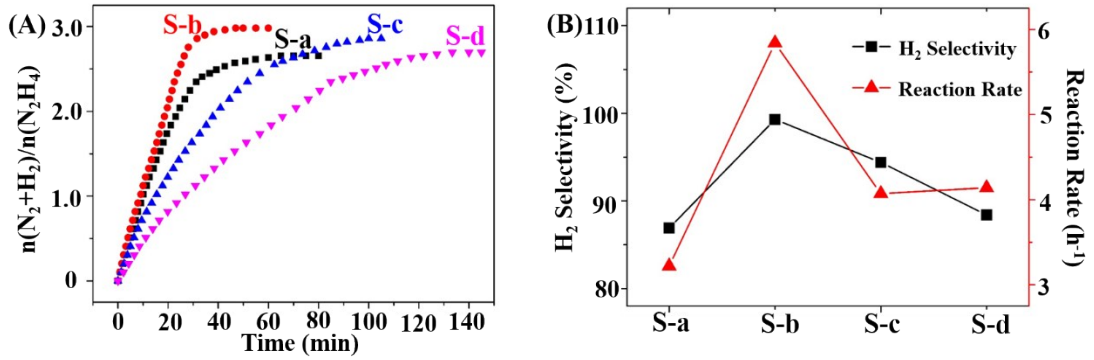

Figure S6. (A) $n(N_2+H_2)/n(N_2H_4)$ versus time for $Ni_{70}Co_{30}/NiO\text{-}CoO_x$ layered nanosheets with different NiCo content prepared by different incomplete precipitation time:10min(S-a), 15min(S-b), 20min(S-c) and 25min(S-d); (B) The variations of H_2 selectivity and reaction rate for $Ni_{70}Co_{30}/NiO\text{-}CoO_x$ layered nanosheets with different NiCo content. (alloy/N_2H_4=1:5, at 25°C)

Figure S6A shows catalytic performance of $NiCo/NiO\text{-}CoO_x$ layered nanosheets with different NiCo content prepared by different incomplete precipitation time, it can be clearly observed that when the incomplete precipitate time is 15min(S-b), the as-attained catalysts present the best catalytic performance. And the variations of H_2 selectivity and reaction rate for these samples are illustrated in Figure S6B, in which S-b has the highest H_2 selectivity and reaction rate than others. Thus the catalyst of $NiCo/NiO\text{-}CoO_x$ layered nanosheets obtained by the incomplete precipitate time of 15min, could harvest the best catalytic activity and selectivity performance.

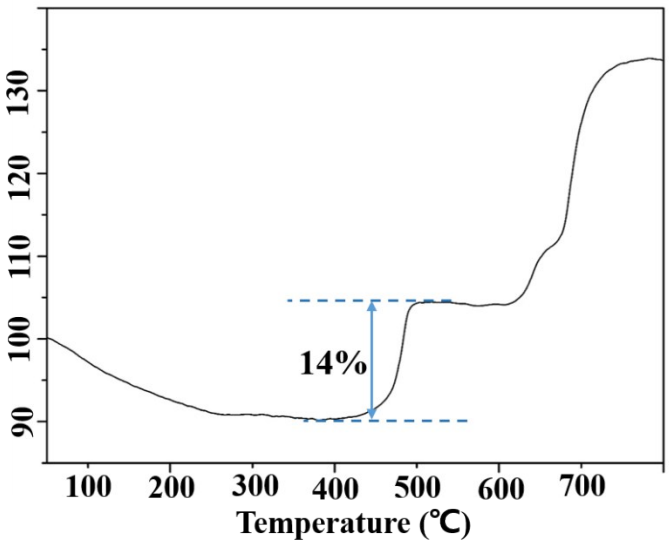

Figure S7. TG analysis for the NiCo/NiO-CoO_x layered nanosheets obtained by the incomplete precipitate time of 15min;

As shown in Figure S7 the TG analysis operated in the air, it can be clearly observed that the weight loss between 50 °C and 200 °C, which could be ascribed to the release of physically adsorbed water. Also, there was a dramatic mass increase of 14% at the temperature range between 200 °C and 500 °C, which corresponded to the NiCo-alloy combined with one oxygen atom. After calculation, it can be obtained that the content of NiCo-alloy is 51.6%. Additionally the mass increase after 600 °C is attributed to NiO and CoO respectively oxidized to Ni_2O_3 and Co_2O_3.

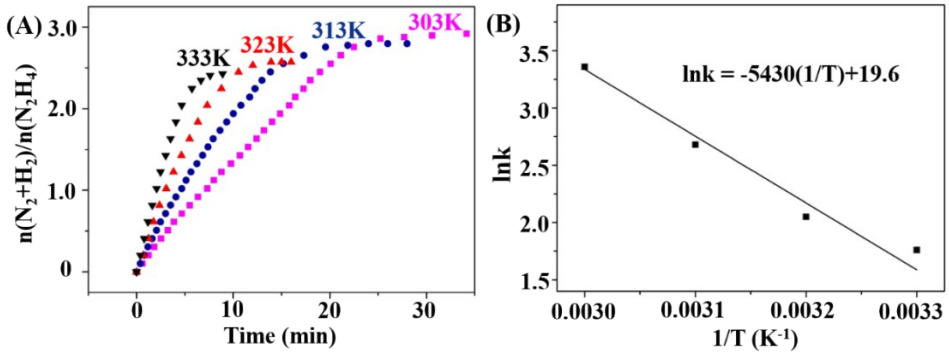

Figure S8. (A) $n(N_2+H_2)/n(N_2H_4)$ versus time for $Ni_{70}Co_{30}$/NiO-CoO_x layered nanosheets at temperatures ranging from 303K, 313K, 323K and 333K. (B) Arrhenius plots for the decomposition of hydrazine catalyzed by $Ni_{70}Co_{30}$/NiO-CoO_x layered nanosheets at different reaction temperatures. (alloy/N_2H_4 =1:5)

In order to obtain the activation energy (Ea) of the H_2 generation from $N_2H_4 \cdot H_2O$ catalyzed by $Ni_{70}Co_{30}$/NiO-CoO_x layered nanosheets, the catalytic reactions were carried out at temperatures ranging from 303 to 333K as show in Figure S8A. It clearly shows that the amount of hydrogen generated is linearly dependent on the reaction time at each temperature, which demonstrates that such a decomposition reaction is of zero order. In a zero-order reaction, the Arrhenius equation can be applied to calculate the Ea of the H_2 generation from $N_2H_4 \cdot H_2O$ catalyzed by the as-synthesized $Ni_{70}Co_{30}$/NiO-CoO_x layered nanosheets. From the Arrhenius plot of lnk versus 1/T in Figure S8B, the Ea is estimated to be 45.15 $kJ \cdot mol^{-1}$, which is lower than most of catalysts reported previously. Additionally, it can be clearly observed that the hydrogen selectivity decreased when increasing the reaction temperature from 303 K to 333 K in Figure S8A. As the coordinated-unsaturated O^{2-} from the ultrathin layered NiO-CoO_x support can weaken the strength of N-H bonds through the hydrogen-bond interaction, thus the cleavage of N-N need more energy than N-H. But the energy of the reaction system will increase when the reaction temperature increased, which would increase the possibility of the cleavage of N-N, thereby decreased the hydrogen selectivity.

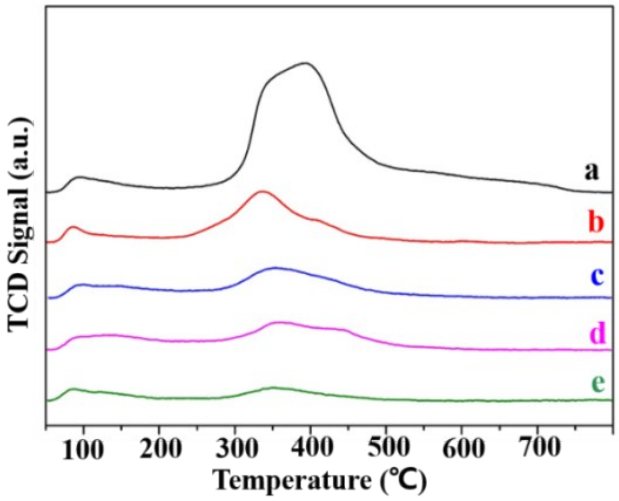

Figure S9. CO_2 TPD profiles of: NiCo/NiO-CoO_x layered nanosheets (a), NiCo/Al_2O_3 (b), urchin-like NiCo/NiO-CoO_x (c), NiCo/NiO-CoO_x NPs (d) and NiCo NPs (e).

A quantitative measure of the number and strength of basic sites was obtained by the CO_2-TPD experiment in Figure S9, it shows that all the samples (curves a–e) can be deconvoluted in two desorption peaks. The peak centered at low temperature (50–120 °C) is generally attributed to the surface hydroxyl groups (weak Brønsted base site); the peak centered at high temperature (300-500 °C) corresponds to the O^{2-} ion with low coordination derived from the surface defects of NiO-CoO_x. Meanwhile, the corresponding value by integral computation of basic strength showed in Table 1, the strength of basic sites on $Ni_{70}Co_{30}$/NiO-CoO_x layered nanosheets was clearly larger than other samples including NiCo/Al_2O_3, urchin-like NiCo/NiO-CoO_x, NiCo/NiO-CoO_x NPs and NiCo NPs, meanwhile the corresponding reaction activity and selectivity were also better than others (Table 1).

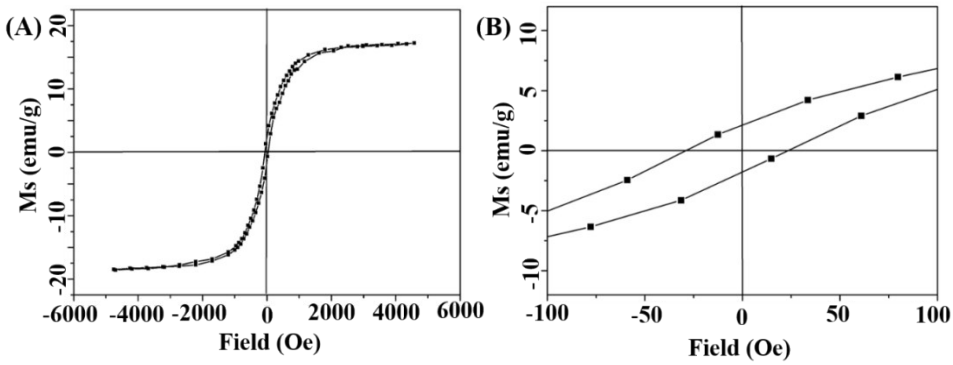

Figure S10. (A) Room-temperature magnetic hysteresis loops of NiCo/NiO-CoO_x layered nanosheets; (B) magnification part hysteresis loops of NiCo/NiO-CoO_x layered nanosheets.

The magnetic hysteresis loop is plotted in Figure S10. As shown in Figure S10A the magnetization saturation (Ms) value is 17.57 emu/g. Although the value is lower than some common magnetic materials, it does not affect the magnetic-recyclability of the products. In our case, the as-prepared NiCo/NiO-CoO_x layered nanosheets suspended in the aqueous solution can quickly respond to a magnet, thus can be easily separated and recovered by an external magnet (Figure 4D inset), and then can be readily redispersed in water by stirring or sonication due to its low coercivity (Hc) (25.17 Oe) and retentivity (Mr) (2.0 emu/g) (Figure S10B), indicating the excellent ability of magnetic separation of NiCo/NiO-CoO_x layered nanosheets.

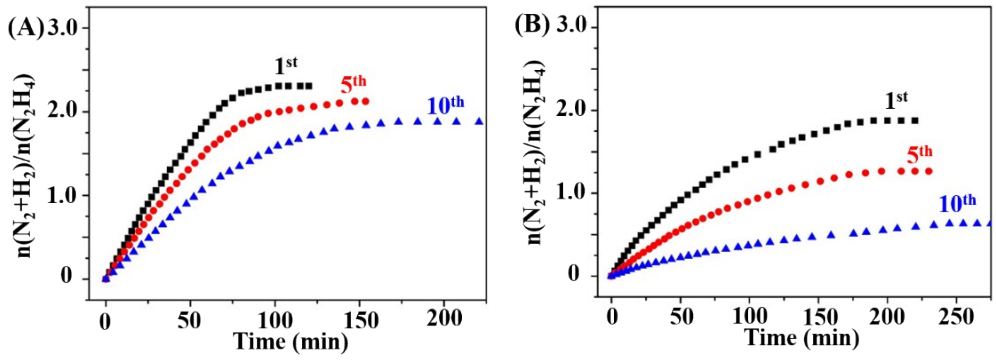

Figure S11. Recyclability tests of $Ni_{70}Co_{30}/NiO\text{-}CoO_x$ nanocomposite for urchin-like spheres (A) and NPs (B). (alloy/N_2H_4 =1:5, at 25°C)

Figure S11 illustrates the lifetime of urchin-like $Ni_{70}Co_{30}/NiO\text{-}CoO_x$ (A) and $Ni_{70}Co_{30}/NiO\text{-}CoO_x$ NPs (B), it can be clearly observed that they both have a greater decrease of activity and selectivity toward the H_2 generation from $N_2H_4{\cdot}H_2O$ decomposition after 10 cycles than those of $Ni_{70}Co_{30}/NiO\text{-}CoO_x$ layered nanosheets showed in Figure 4D, especially $Ni_{70}Co_{30}/NiO\text{-}CoO_x$ NPs.